

A Performance Investigation of Receive Beamforming Schemes in Specular Tissue Characterization

Gayathri Malamal and Mahesh Raveendranatha Panicker
Center for Computational Imaging, Dept. of Electrical Engineering
Indian Institute of Technology Palakkad, Kerala, India
121814001@smail.iitpkd.ac.in; mahesh@iitpkd.ac.in

Abstract—This work presents a comparison of the delay and sum (DAS), filtered delay multiply and sum (DMAS), minimum variance (MV) and specular receive beamforming schemes in the context of ultrasound imaging of specular reflectors. The main contributions of the study are, 1) a performance comparison of the four receive beamforming schemes through experimental studies for varying angulations of planar reflectors and for reflectors located at varying depths in the medium and, 2) an investigation on the influence of the sub-array length in MV beamforming on the imaging of specular structures. The qualitative conclusions are quantitatively validated in terms of contrast and generalized contrast-to-noise ratios. The study examines the benefits and drawbacks of each receive beamforming technique and highlights the significance of application-tailored beamforming schemes for imaging specular structures.

Index Terms—beamforming, needle guidance, specular reflection, ultrasound

I. INTRODUCTION

Ultrasound (US) imaging typically employs the pulse-echo approach of imaging where the backscattered signals that are received by the transducer are beamformed to reconstruct the final image. The popular receive beamforming schemes in US imaging include the delay and sum (DAS) [1], filtered delay multiply and sum (DMAS) [2], and the minimum variance (MV) beamforming [3] schemes. However, these receive beamforming schemes assume the medium to be homogeneous and diffuse which gets violated in the presence of specular reflections. The specular reflections occur from structures of dimensions much greater than the ultrasonic wavelength and have high intensity and directivity that is governed by the angle of incidence of the ultrasound wavefront and the reflector orientation. A specular beamforming (SB) scheme dedicated to imaging of specular structures has also been proposed in literature [4]. Contrary to DAS, DMAS and MV, SB utilizes the principles of Snell's law for beamforming and specifically enhances the visualization of the specular reflectors. Nevertheless, there is hardly a comparative study to examine the performance of receive beamforming schemes in the context of imaging specular structures.

This work is supported by Department of Science and Technology - Science and Engineering Research Board (DST-SERB ECR/2018/001746) and the Ministry of Education, India.

This paper aims to address this gap by comparing and contrasting the performance of DAS, DMAS, MV and, SB schemes for specular imaging. The study investigates specular reflectors at varying angulations and depths and also examines the influence of sub-array length (L_s) in the MV approach for specular imaging. The paper is structured as follows. Section II describes the four beamforming schemes and the experimental setup. The results are presented in Section III and the associated discussion in Section IV.

II. METHODS

A. Delay and Sum Beamforming (DAS)

In DAS, the delay compensated signals from all the transducer elements are apodized and summed to form the final beamformed signal, y_{DAS} , after coherent compounding across the T transmissions with uniform angular apodization as (1),

$$y_{DAS}(P) = \sum_{j=1}^T \sum_{i=1}^{N_c} W_i(P) s_i(\tau_P(i, j)) \quad (1)$$

where, $s_i(\tau_P(i, j))$ represents the delay compensated signal, $W_i(P)$ is the apodization weight of the i^{th} transducer element which is proportional to its geometric distance to the pixel P . This is because the conventional DAS assumes a diffusive homogeneous medium and is independent of the received data [1]. Apodization functions such as rectangular, Hamming, Hanning, Tukey, or Gaussian weighted windows are typically used in DAS where, the center of the window is decided by defining an accurate F - number for the transducer considering the directivity of elements [1].

B. Delay Multiply and Sum Beamforming (DMAS)

The DMAS is a non-linear beamforming algorithm that has been introduced to overcome some of the limitations introduced by DAS [2] by leveraging the coherence in the received data. The delay compensated signals are initially pairwise multiplied in all possible combinations (excluding self-product terms) before summation to form the beamformed signal y_{DMAS} expressed as (2),

$$y_{DMAS}(P) = \sum_{j=1}^T \sum_{i=1}^{N_c-1} \sum_{k=i+1}^{N_c} s'_i s'_k \quad (2)$$

where,

$$s'_i = \text{sign}(s_i) \sqrt{|s_i(\tau_P(i, j))|} \quad (3)$$

$$s'_k = \text{sign}(s_k) \sqrt{|s_k(\tau_P(k, j))|} \quad (4)$$

where, s_i, s_k are the delay compensated signals from the i^{th} and $(i+1)^{\text{th}}$ array elements respectively. The multiplication of signals with similar frequency content synthetically generates a baseband and second harmonic in the spectrum, from which the second harmonics are extracted and filtered with a band-pass filter to obtain the filtered DMAS beamformed signal to improve lateral resolution and contrast.

C. Minimum Variance (MV) Beamforming

In MV beamforming, the aperture weights are data-dependent and are adaptively estimated from the signals received in the transducer elements. It aims to improve the resolution through the suppression of off-axis signals and allowing the side lobes in the directions with minimum energy [3]. The beamformed signal (y_{MV}) is expressed in vector form with a time-dependent complex apodization weight W for each transmission j as (5),

$$y_{MV}(P, j) = W(P)^H s(P, j) \quad (5)$$

The receive beamforming with MV is viewed as an optimization problem that minimizes the variance or the power of y_{MV} while imposing unit gain in the focal point or the intended direction (distortionless response) and treating all the other signals as interference or noise [3]. The optimization problem is formulated as (6), where a refers to the steering vector, which is a vector of ones for the delay compensated aperture data,

$$\min_{W(P)} (W(P)^H R(P) W(P)) \quad \text{subject to } W(P)^H a = 1 \quad (6)$$

$$R(P) = E[s(P)s(P)^H] \quad (7)$$

where, $E[\cdot]$ denotes the expectation operator and $R(P)$ represents the spatial covariance matrix estimated as (7). The analytical solution to (6) is the adaptive weight vector (8) that is applied to obtain the beamformed signal in (5).

$$W(P) = \frac{R(P)^{-1} a}{a^H R(P)^{-1} a} \quad (8)$$

D. Specular Beamforming

The specular beamforming SB [4] is a dedicated beamforming to enhancing specular reflections. It leverages the adherence of specular reflections to Snell's law to develop a specular transform that maximizes the detection of specular patterns in the received data. The specular beamformed signal (termed as specular transform in [4]), y_{SB} is represented as (9), where the propagation delay is a function of transmit (α_j) and receive (α_r) (and thereby on the reflector orientation α_g) angles.

$$y_{SB}(P, \alpha_g) = \sum_{j=1}^T s(\tau_P(\alpha_j, \alpha_j - 2\alpha_g)) \quad (9)$$

TABLE I
COMPARISON OF CR, AND gCNR

α_g (°)	DAS/DMAS/MV/SB	
	CR(dB)	gCNR
20	-0.80/13.61/18.46/ 26.8	0.47/0.90/ 0.99/0.98
30	-3.40/9.61/8.7/ 19.8	0.51/0.68/0.78/ 0.92
0 (4.3 mm)	27.92/7.11/24.38/ 29.68	1/0.79/0.98/0.98
0 (17.5 mm)	30.62/24.89/24.97/ 33.61	1/1/1/1

The work also proposes to enhance the signal-to-noise ratio and the reflection detection probabilities further by correlating the specular transformed signals with a matched filter model, derived to maximize the specular energy. Nevertheless, the method suppresses diffuse reflections and therefore needs to be supplemented with other beamforming techniques.

E. Experimental Setup

Three datasets are acquired with Verasonics Vantage US research platform using L11-5v transducer for 73 plane-wave(PW) transmissions in the range $[-18^\circ, +18^\circ]$. The first dataset is obtained by inserting a 15G needle into the gel phantom for needle orientations $\alpha_g = 20^\circ$, and 30° . Furthermore, a dataset is acquired by inserting a 15G stainless steel needle parallel to the transducer at a depth of 4.3 mm in the uniform gel medium. Another dataset is acquired by inserting the same needle at a depth of 17.5 mm in the same gel medium. All the datasets are later added with speckle noise. The imaging performance is compared against DAS using contrast ratio (CR), and generalized contrast-to-noise ratio (gCNR). Furthermore, two additional *in-vitro* datasets are acquired to compare the beamforming schemes for imaging specular reflectors located at different depths.

The beamformed images are reconstructed from the RF datasets using MATLAB R2019a (The MathWorks, Natick, MA, USA) through coherent PW compounding. The MV beamforming is performed with $L_s = 32$, for a temporal sample size of size 5, and a diagonal loading parameter of $1/10^8$. Further, a comparative study with MV beamforming of $L_s = 8$ and 64 is also performed. The images are shown for a dynamic range of 60 dB.

III. RESULTS

Row 1 in Fig. 1 are the beamformed images for $\alpha_g = 20^\circ$, and row 2 for $\alpha_g = 30^\circ$ with the DAS, filtered DMAS, MV, and SB schemes respectively arranged along columns 1, 2, 3, and 4. The reflector is better visualized in PW images with filtered DMAS, MV, and SB when compared to the PW-DAS images where the reflector is significantly degraded by the speckle noise. The quantitative metrics CR, and gCNR, are presented in the Table I to confirm the qualitative conclusions. The beamforming schemes are compared for their performance in imaging specular reflectors at two different depths in Fig. 2. Fig. 2(a)-(d) show respectively the DAS, filtered DMAS, MV, and SB images for the needle at a depth of 4.3 mm in the

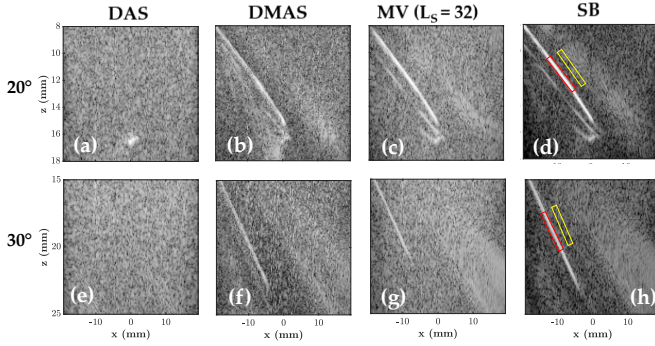


Fig. 1. Beamformed images of the needle inserted into the gel phantom at 20° (a) DAS (b) DMAS (c) MV and (d) SB. At 30° (e) DAS (f) DMAS (g) MV and (h) SB.

gel phantom. The performance of filtered DMAS is severely degraded as the reflector is hardly visible when compared to the other beamforming schemes. The spatial distribution of the reflected energy from a pixel located on the specular reflector is plotted in Fig. 2(e). The x axis indicates the PW transmissions between $[-18^\circ, +18^\circ]$, and the y axis is the range of angles (α_r) made by the pixel with each of the N_c transducer elements. The plot shows that only a few elements that are closer to the pixel of interest ($\alpha_r = 0^\circ$) are receiving the reflected energy across the PW transmissions. It is also noted that DAS and SB images in Fig. 2(a) and (d) resolve the reflector better towards the edges of the scan grid (between $x = -15$ mm to -10 mm and $x = 10$ mm to 15 mm). However, when the reflector is at a greater depth of 17.5 mm, DMAS in Fig. 2(g) is of comparable visual quality to DAS, MV and SB images in Fig. 2(f), (h) and, (i) respectively. Contrary to the previous case, the plot of the spatial distribution of reflected energy from the pixel on the reflector in (Fig. 2(j)), shows that more transducer elements receive the reflections. A small discontinuity exists in the reflector between $x = 5$ mm - 12 mm which is due to the air content in the gel medium during the experiment and is captured in the DAS, DMAS, and SB images, but is not very evident in the MV image (Fig. 2(h)). The quantitative metrics for the two cases are presented in Table I (last two rows). The specular ROI is selected on the needle and the background region is selected just outside the needle as annotated in the SB images in Fig. 2 in red and yellow respectively. Interestingly, in both cases, the DAS shows comparable metric values with SB and higher metric values consistently over DMAS and MV beamforming.

Finally, the influence of L_s in MV beamforming on the imaging of specular reflectors are analysed and presented in Fig. 3. The MV beamformed images reconstructed with $L_s = 64$ in row-1 and with $L_s = 8$ in row-2 of Fig. 3. It is seen that the performance of MV in imaging the specular reflectors is adversely affected by $L_s = 64$ when compared to the corresponding images for $L_s = 32$ and 8. The needle appears distorted with only a small section of the structure visible in the beamformed images. For $L_s = 8$, the needle structures are enhanced particularly at the entry point and the

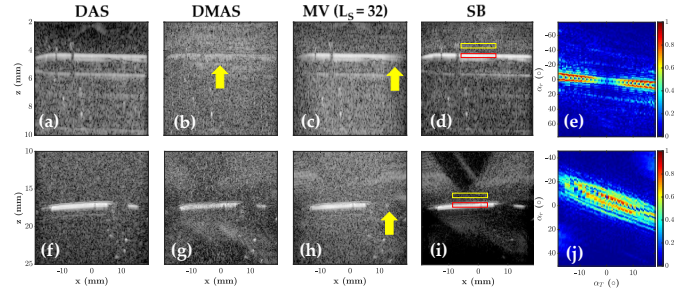


Fig. 2. Comparison of the beamforming schemes for needle at a depth of 4.3 mm (a) DAS (b) DMAS (c) MV (d) SB. (e) Distribution of the reflected energy from a pixel located at $(x, z) = (0.45, 4.3)$ mm. For needle at a depth of 17.5 mm (f) DAS (g) DMAS (h) MV (i) SB and (j) Distribution of the reflected energy from a pixel located at $(x, z) = (-1.6, 17.5)$ mm.

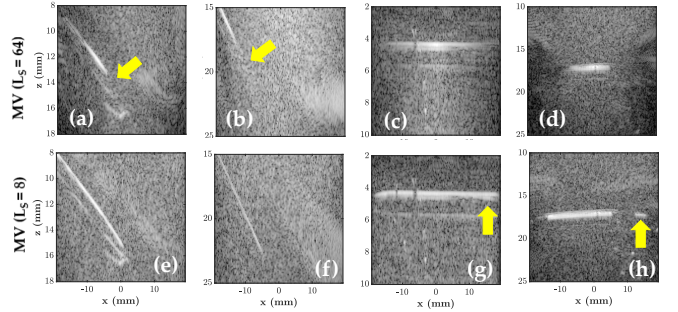


Fig. 3. MV beamformed images with $L_s = 64$ for the needle inserted into the gel phantom at (a) 20° and (b) 30°. For the needle at 0° at a depth of (c) 4.3 mm and (d) 17.5 mm. MV beamformed images with $L_s = 8$ at (e) 20° and (f) 30°. For the needle at 0° at a depth of (g) 4.3 mm and (h) 17.5 mm.

tip of the needles when compared to $L_s = 32$ in Fig. 1. Further, in Fig. 3(g), it is seen that the reflector is better resolved towards the edges of the scan grid (between $x = -15$ mm to -10 mm and $x = 10$ mm to 15 mm). Similarly, the small discontinuity in the reflector which is not very evident in Fig. 2(h) is captured with $L_s = 8$ in Fig. 3(h).

IV. DISCUSSION

This paper compared the DAS, DMAS, MV, and specular beamforming techniques in the imaging of planar specular structures for PW transmissions. The study focused on validating the receive beamforming schemes for various orientations and depths of the structures relative to the transducer array. Additionally, the study evaluated the significance of choosing L_s appropriately for imaging specular surfaces with MV beamforming. The results indicate that the DMAS, MV, and SB techniques outperform DAS beamforming in imaging specular reflectors at different reflector angles. This is because the DMAS and MV beamforming techniques do not rely on a data-independent/geometry-driven apodization like DAS whereas SB leverages the physics of specular reflections to exclusively image the specular reflectors.

In DMAS beamforming, the apodization is inherent from the pair-wise multiplication of signals received by the transducer elements [2]. The multiplication is effectively an autocor-

relation of the receive aperture in the reflections received across the transducer array elements. As a result, the pairwise multiplication emphasizes the contribution of specular reflections due to coherence enhancement by auto-correlation in the beamformed signal, even when reflections from inclined reflectors are reflected off-axis based on the angle of incidence of the PW transmission. When comparing different beamforming schemes for imaging specular reflectors at varying depths, DMAS underperforms DAS, MV beamforming, and SB, especially at shallower depths closer to the transducer (as shown in Fig. 2(a)-(d)). This is because reflections are received only by the transducer elements closest to the reflector pixels due to the limited range of reflection angles at these depths, as illustrated in Fig. 2(e). The inherent auto-correlation of the aperture in DMAS, which is expected to improve coherence, contributes to clutter due to minimal reflections available in the farther transducer elements. Consequently, the geometry-driven apodization in DAS is ideal and is a suitable candidate for shallow-depth applications. However, when the reflector is at a greater depth (Fig. 2(f)-(i)), the performance of DMAS is improved as the reflected energy is available in more transducer elements as seen in Fig. 2(j).

The MV beamforming with $L_s = 32$ gives a consistent performance in all cases when compared to DAS and DMAS. However, a slight deterioration of the image quality of the reflectors is observed at the edges of the scan grid in Fig. 2. This is because the MV approach assumes sufficient signal-to-noise ratio in the subarrays which may be minimal from the pixels closer to the edges of the scan plane. A smaller subarray length is more optimal towards the edges of the scan grid. The performance of MV beamforming while imaging specular structures is adversely affected when L_s is not selected correctly. Typical adaptive beamforming schemes like MV seek to minimize the variance in the received data to determine the best set of receive aperture weights to improve contrast and resolution. The optimal L_s for the minimization problem is proposed as $L_s \leq N_c/2$. A smaller $L_s \in [1, N_c/2]$ improves the robustness by trading off the resolution and higher L_s improves the resolution by compromising robustness. Nevertheless, the results presented in Fig. 3 illustrated that an enhanced visualization of the specular structures is subjected to choosing correct $L_s \in [1, N_c/2]$. A $L_s = 64$ worsens and a $L_s = 8$ enhances the output of MV in the context of specular imaging. This is because the reflected energy from the specular reflector is concentrated on a few transducer elements, unlike the diffuse scattering where the scattered signals are spatially distributed across the transducer array. It is found that the reflected specular energy approximately is distributed within 32 transducer elements, therefore a $L_s > 32$ accumulates noise during the estimation of spatial covariance. However, the selection of optimal L_s for enhancing specular reflectors should not compromise the resolution and contrast of the soft tissue structures. A smaller L_s as 8 degrades the resolution of soft tissue structures when compared to $L_s = 64$. Therefore, an optimization framework needs to be developed to tune L_s according to the imaging scenario. This can add to

the existing computational complexity of MV.

Upon analyzing the performance of SB, it is found to be superior to all other beamforming techniques. However, as anticipated, the improvement is focused on specular structures, resulting in the suppression of soft tissue structures (i.e., non-specular structures). This is not ideal for real-time imaging, as the suppression of such tissue structures can lead to the loss of crucial tissue information (such as missing important anatomical landmarks) and create diagnostic challenges.

It is emphasized that all the discussed receive beamforming techniques have their unique advantages, but also have limitations while imaging specular interfaces. Hence, it is not feasible to directly apply any of these techniques for imaging specular structures without considering the application.

ACKNOWLEDGMENT

The authors would like to acknowledge the facilities of the Center for Computational Imaging, Indian Institute of Technology Palakkad (IITPKD), India, and Mr. Ananthu Sasikumar, Junior Technician, IITPKD for his assistance in logistics.

REFERENCES

- [1] V. Perrot, M. Polichetti, F. Varray, and D. Garcia, "So you think you can DAS? A viewpoint on delay-and-sum beamforming," *Ultrasonics*, vol. 111, p. 106309, 3 2021.
- [2] G. Matrone, A. S. Savoia, G. Caliano, and G. Mageses, "The delay multiply and sum beamforming algorithm in ultrasound B-mode medical imaging," *IEEE Transactions on Medical Imaging*, vol. 34, no. 4, pp. 940–949, 4 2015.
- [3] J. F. Synnevåg, A. Austeng, and S. Holm, "Adaptive beamforming applied to medical ultrasound imaging," *IEEE Transactions on Ultrasonics, Ferroelectrics, and Frequency Control*, vol. 54, no. 8, pp. 1606–1613, 8 2007.
- [4] A. Rodriguez-Molares, A. Fatemi, L. Lovstakken, and H. Torp, "Specular Beamforming," *IEEE Transactions on Ultrasonics, Ferroelectrics, and Frequency Control*, vol. 64, no. 9, pp. 1285–1297, 9 2017.